J. Phys. Chem. A **2008,** *112,* 3133−3140 **3133**

ReaxFF Reactive Force Field for Solid Oxide Fuel Cell Systems with Application to Oxygen Ion Transport in Yttria-Stabilized Zirconia

Adri C. T. van Duin, Boris V. Merinov, Seung Soon Jang, and William A. Goddard III*

Materials and Process Simulation Center (139-74), California Institute of Technology, Pasadena, California 91125

Received: August 23, 2007; In Final Form: November 21, 2007

We present the ReaxFF reactive force field developed to provide a first-principles-based description of oxygen ion transport through yttria-stabilized zirconia (YSZ) solid oxide fuel cell (SOFC) membranes. All parameters for ReaxFF were optimized to reproduce quantum mechanical (QM) calculations on relevant condensed phase and cluster systems. We validated the use of ReaxFF for fuel cell applications by using it in molecular dynamics (MD) simulations to predict the oxygen ion diffusion coefficient in yttria-stabilized zirconia as a function of temperature. These values are in excellent agreement with experimental results, setting the stage for the use of ReaxFF to model the transport of oxygen ions through the YSZ electrolyte for SOFC. Because ReaxFF descriptions are already available for some catalysts (*e.g.*, Ni and Pt) and under development for other high-temperature catalysts, we can now consider fully first-principles-based simulations of the critical functions in SOFC, enabling the possibility of *in silico* optimization of these materials. That is, we can now consider using theory and simulation to examine the effect of materials modifications on both the catalysts and transport processes in SOFC.

1. Introduction

Zirconia (ZrO_2)-based ceramics play an important role in many technological applications. In its pure form zirconia has limited mechanical applications because of structural polymorphism inherent to this compound. The low-temperature form is monoclinic, space group $C_{2h}^{5} = P2_1/c$, which transforms to the tetragonal phase (space group $D_{4h}^{15} = P4_2/nmc$) at $T \sim 1440$ K, and then to the cubic fluorite phase (space group $O_h^5 = Fm3m$) at $T \sim 2640$ K. However, alloying zirconia with various metal oxides such as CaO, MgO, La_2O_3, Sc_2O_3, and Y_2O_3 stabilizes the cubic fluorite phase, which significantly improves its thermomechanical properties. Typical characteristics of stabilized zirconia include excellent strength, toughness, wear resistance, high-temperature stability, and corrosion resistance. In addition, many of these systems have superionic conductivity at high temperature, leading to applications as oxygen sensors and as membranes for high temperature solid oxide fuel cells (SOFCs). In particular, Y_2O_3 doping (∼8 mol %, denoted as YSZ-8) leads to highly mobile anion vacancies, providing an ionic conductivity of $\sim 10^{-1}$ $S \cdot cm^{-1}$ at 1000 °C.[1]

Extensive experimental and theoretical studies have been reported for YSZ, but the description of the atomistic mechanism underlying the increased stabilization, the interaction between defects, and the locations of the oxygen vacancies relative to the dopant atoms remain uncertain. Indeed, no reliable microscopic mechanism for the phase transitions has been proposed for doped ZrO_2. In addition, many results reported about the structural properties of stabilized zirconia are incomplete or contradictory. For instance, even the simplest question of the location of the O vacancy (V_O) relative to the Y dopant is controversial. Thus some papers suggest that the vacancy lies in a nearest neighboring (NN) position to Y,[2−6] whereas others report the vacancy to be next (second) nearest neighbors (2NN) to the Y.[7−12]

We expect that determining the atomistic mechanism underlying the properties of YSZ might suggest changes in the materials and processing to optimize the properties. Unfortunately, the available means of experimentally characterizing these systems provides little guidance for improving them. Experiments have provided overall estimates of some relevant quantities, but it is most difficult to determine experimentally the atomistic structural details needed to postulate and test mechanistic ideas.

To make progress with such limited experimental data, it is essential to use first-principles-based molecular dynamics and Monte Carlo simulations. However, first principles simulations of reactions has usually meant quantum mechanics (QM, solving the Schrödinger equation), which is not practical for systems with the large periodic cells (>1000 atoms) and time scales (>10 ns) required for studying diffusional properties in YSZ. QM[13−15] and pseudopotential-based molecular dynamics (MD)[16] have been reported for YSZ, but length and time scales were too small to examine the issues relevant to improving the properties of YSZ.

The development of the ReaxFF reactive force field provides a means to enable such long-term MD on the large-scale complex systems relevant for YSZ. ReaxFF is based fully on accurate QM and retains nearly the accuracy of QM while allowing large scale MD for computational costs nearly as low as for simple force fields. ReaxFF has been applied to reactive processes for many systems including organic reactions,[17] reactions of energetic materials under extreme conductions,[18,19] decomposition of improvised explosive devices,[20] thermal decomposition of polymers,[21] selective oxidation of propene by $BiMoO_x$ heterogeneous catalysts,[22] catalysis at fuel cell electrodes and proton conductivity of PEM,[23] crack propagation in silicon crystals,[24] dissociation of H_2 on Pt surfaces,[25] hydrogen

---

* Corresponding author. E-mail: wag@wag.caltech.edu.

10.1021/jp076775c CCC: $40.75

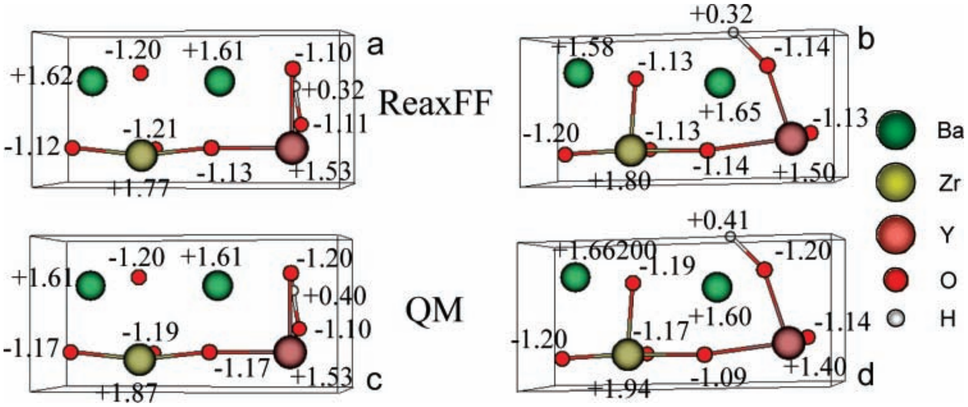

Figure 1. ReaxFF (a, b) and QM (c, d) charges for two configurations of a 25% YH-exchanged $BaZrO_3$ condensed phase.

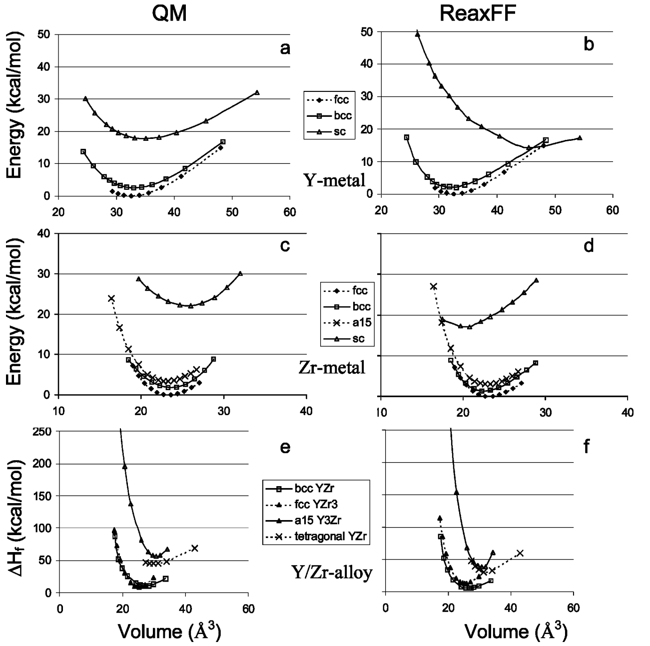

Figure 2. QM- and ReaxFF equations of state for various polymorphs of the Y metal (a,b), Zr metal (c, d) and Y/Zr alloys (e, f).

storage in Mg nanoclusters,[26] catalytic formation of carbon nanotubes,[27] tribology of metal−metal oxide interfaces.[28] Recently, we used ReaxFF to investigate the initial steps of oxidation of O_2 with aromatic and aliphatic systems,[29] showing that ReaxFF may be applied to complex oxidations.

Particularly important features of the ReaxFF reactive force fields are that

- it allows partial covalency to be included with the bond order and bond strength varying continuously with distance
- it allows the charges on the atoms to vary continuously with coordination and bond order,
- the parameters are based solely on QM descriptions of both reactive processes and equations of state, allowing an iterative refinement of ReaxFF to handle any unusual bonding interactions encountered in the applications.

Here, we describe the development of the ReaxFF force field for materials containing Y, Zr, and O, which we apply to MD simulations of oxygen diffusion in Y-stabilized ZrO_2. The results are in excellent agreement with experiment, validating the use of ReaxFF for studying the transport properties of these membranes. This enables the study of oxygen transport under realistic conditions as it is generated at the cathode, migrates through the membrane, and reacts with fuel at the anode. Because ReaxFF can also be used to describe the chemical processes on the anode and cathode and the migration of ions across the electrode-membrane interface, ReaxFF opens the door to practical atomistic first principles predictions on models of a complete fuel cell that include realistic descriptions of the various interfaces and processes.[23]

Section 2 describes the computational details of the simulations, and section 3 describes the ReaxFF reactive force field for systems containing Y, Zr, and O. Section 4 then examines the application to issues related to O diffusion in YSZ. These studies focus on validation, for modest sized systems and modest periods. However, ReaxFF calculations on multiprocessor clusters have been reported for reactive processes on systems with 1 000 000 atoms[30] with time scales of hundreds of nanoseconds.

2. Computational Details

All QM calculations were performed at $T = 0$ K using the generalized gradient approximation (GGA)[31,32] to density functional theory (DFT).[33] The PBE functional[34] was employed for the periodic calculations, and the hybrid B3LYP functional was used for the finite cluster calculations. B3LYP combines exact Hartree−Fock exchange with the local exchange functional of Slater[35] and includes the Becke nonlocal gradient correction,[36] the Vosko−Wilk−Nusair exchange functional,[37] and the Lee−Yang−Parr local and nonlocal correlation functional.[38] The accuracy of these and other DFT methods is summarized in refs 39 and 40.

The Jaguar 4.2 program package[41] was employed for the ab initio cluster calculations. The Y and Zr metals were described by the Hay and Wadt core−valence relativistic effective core potentials (ECP) or pseudopotentials (PP)[42] with the LACVP** basis set of the Jaguar program package. This nonlocal ECP uses angular momentum projection operators to enforce the Pauli principle.[43,44] The oxygen atoms were described at the all-electron level using the variant of the Pople 6-31G** basis set,[45] in which the six d Gaussians were reduced to the five with angular momentum 2.

The periodic QM calculations were carried out using the SeqQuest code,[46,47] which uses Gaussian basis functions rather than the plane wave basis often used in periodic systems. Nonlocal ECP or PP,[44,48] similar to those in ref 43 but for use in periodic systems were employed to replace the core electrons. These calculations used double-zeta plus polarization contracted Gaussian functions[47] optimized for periodic calculations.

These QM results obtained for relevant condensed phases and cluster systems were then used to derive parameters for the ReaxFF as described in section 3, which was subsequently used in the MD simulations described in section 4.

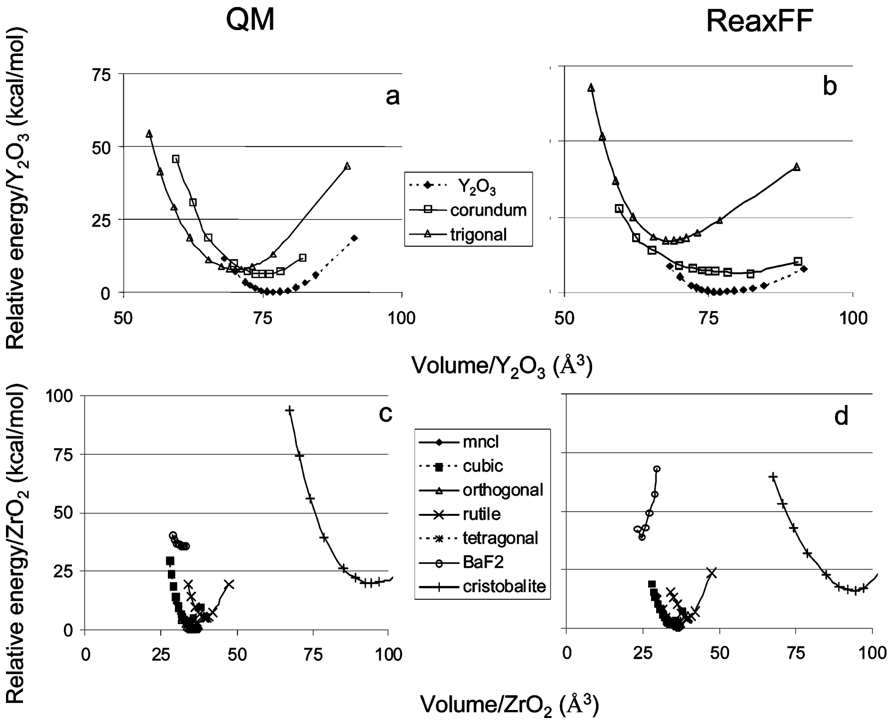

Figure 3. QM- and ReaxFF equations of state for various polymorphs of Y_2O_3 (a, b) and ZrO_2 (c, d).

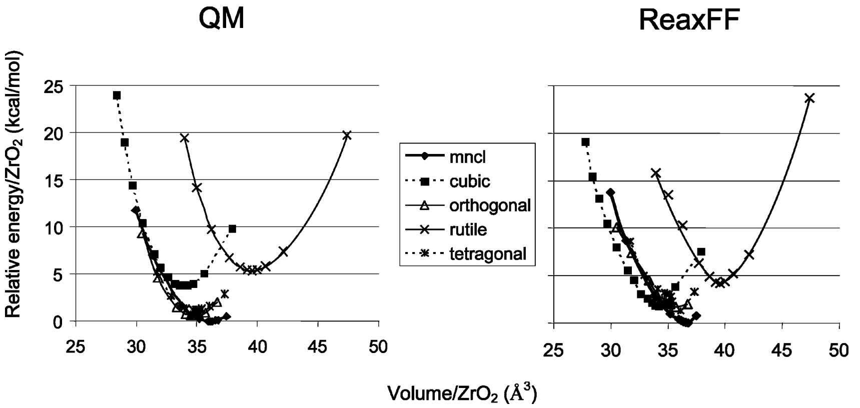

Figure 4. QM- and ReaxFF equations of state for the low-energy ZrO_2 polymorphs.

3. ReaxFF Development

To develop a reliable ReaxFF description for simulating reactive oxygen migration in Y-stabilized ZrO_2-phases, we performed periodic QM-simulations on a range of systems. The main focus of these QM-simulations was on bulk and surface oxide systems to enable future ReaxFF applications involving reduction reactions at YZrO surfaces. Because such processes may result in the formation of metallic phases, we also included in the ReaxFF training set the unoxidized periodic metals: Y, Zr, and the Y/Zr alloys.

To determine the parameters for ReaxFF, we carried out QM calculations for the following systems:

- The Mulliken charge populations for several phases of Y_2O_3, ZrO_2, and $BaZr_{0.75}Y_{0.25}OH_{0.25}$. This latter case was included to allow applications to hydrogen transfer in YH-exchanged $BaZrO_3$ phases. These charges shown in Figure 1 were used to determine the electronegativity, hardness, and radius parameters that go into the charge calculation part of ReaxFF. For the cubic ZrO_2 bulk phase, ReaxFF calculates a charge of +1.99 on the Zr, compared to a QM/Mulliken charge of +2.5. For the Y_2O_3 phase, ReaxFF calculates a charge of +1.60 on the Y, compared to a QM/Mulliken charge of +1.86.
- The equations of state for the fcc, bcc, and simple-cubic (sc) phases of Y metal (Figure 2a, b) and the fcc, bcc, A15, and sc phases of Zr metal (Figure 2c, d). For the Y/Zr alloys, we considered the YZr bcc and tetragonal phases, the fcc phase for YZr_3, and the A15 phase of YZr_3 (Figure 2e, f). These calculations include coordination numbers ranging from 6 to 12, ensuring that ReaxFF is able to predict correctly the coupling of energy with coordination and bond order. Here we considered volumes up to 10% above equilibrium down to 30% below equilibrium, which spans a pressure range of −10 GPa (tension) to +25 GPa (compression). This provides the data to ensure that effects of Pauli repulsion are described well, plus it provides data for changes in bond order and long-range attraction.
- The equations of state from QM and ReaxFF for various phases of ZrO_2, Figures 3 and 4. Here we include the cubic high-temperature form (the fluorite structure for $T > 2640$ K) with 8 O neighbors to each Zr and the monoclinic form with 7 O neighbors to each Zr and 4/3 Zr neighbors for each O. For this equation of state, we fixed the monoclinic angle at $\beta = 99.123°$ and optimized the three remaining cell parameters for pressures ranging from −5 to +30 GPa). In addition, we included other phases involving the same composition: rutile

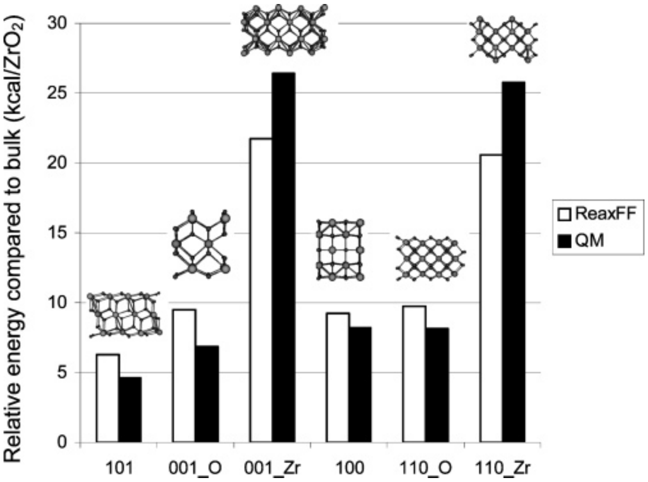

Figure 5. QM- and ReaxFF surface energies for the orthorhombic (space group *Pbca*) ZrO_2 phase. In each case the surface is at the top.

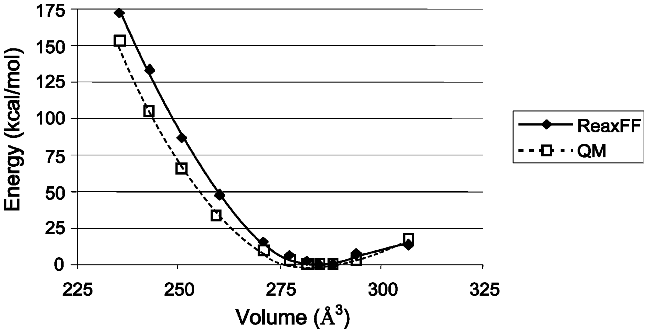

Figure 6. QM- and ReaxFF equations of state for a YSZ-14 phase $[(Y_2O_3)(ZrO_2)_6]$.

(6-coordinate Zr with $c/a = 0.67192$ optimized for zero pressure), orthorhombic (7-coordinate Zr and 4/3-coordinate O, $c/a = 0.5045$), tetragonal (8-coordinate Zr, $c/a = 1.4601$), BaF_2-type (9-coordinate Zr with 6/3-coordinate O, $c/a = 1.6579$), and cubic SiO_2-cristobalite structures (4-coordinate Zr and 2-coordinate O). Fitting ReaxFF to this range of coordination numbers ensures it can predict correctly the coupling of energy with coordination, bond order, and angle energy terms.

- The equation of state for various phases of Y_2O_3. (Figure 3). Here the only experimental structure has space group $T_h^7 = Ia\bar{3}$ with 6-coordinate Y. We include also the corundum structure (space group $D_{3d}^6 = R\bar{3}c$) with 6-coordinate Y and the trigonal La_2O_3-type structure (space group $D_{3d}^3 = P\bar{3}m$), which has 7-coordinate Y and 6(33%)/4(66%)-coordinate O.
- The surfaces energies for various surfaces of the orthorhombic phase of ZrO_2, Figure 5.
- The equation of state for the $[(Y_2O_3)(ZrO_2)_6]$ system with 14.3 mol % mixed oxide (YSZ-14), Figure 6. The O vacancy was placed into two different 2NN positions relative to the Y.
- Relative energies for various distributions of Y and the O vacancy for the $[(Y_2O_3)(ZrO_2)_{14}]$ system with 7.1 mol % alloy (YSZ-7), Figure 7. Here we varied the positions for O vacancy, putting it in various NN, 2NN, and 3NN (the third nearest neighboring) positions relative to the Y. To provide data describing the relative locations of the Y atom and the O vacances, we considered six distinct distribuions for YSZ-7:

(1) configuration 1 has one of the two Y atoms in a NN position and the other in a 2NN position to the O vacancy with $\angle Y_1V_OY_2 \sim 150°$;

(2) configuration 2 has both Y atoms in 2NN positions to the O vacancy with $\angle Y_1V_OY_2 \sim 150°$;

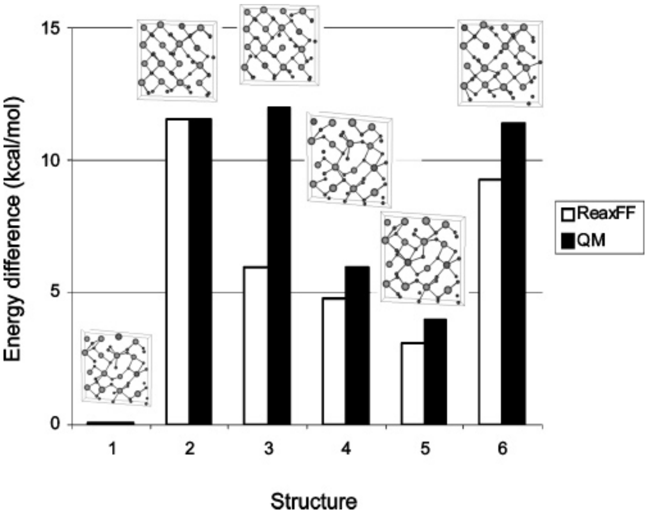

Figure 7. QM- and ReaxFF energies for six configurations of a YSZ-7 phase $[(Y_2O_3)(ZrO_2)_{14}]$.

(3) configuration 3 has both Y atoms in 2NN positions but with $\angle Y_1V_OY_2 \sim 115°$;

(4) configuration 4 has one of the two Y atoms in a NN position and the other in a 2NN position to the O vacancy but with $\angle Y_1V_OY_2 \sim 110°$;

(5) configuration 5 has again one of the Y atoms in a NN position and the other in a 2NN position with $\angle Y_1V_OY_2 \sim 115°$, but orientation of the $Y_1V_OY_2$ fragment differs from that in configuration 4 approximately by 90°;

(6) configuration 6 has both Y atoms in 3NN positions to the O vacancy.

Figures 1−7 compare the acccuracy of the final ReaxFF in reproducing these various QM reuslts. The complete set of parameters used in these simulations is in the Supporting Information.

4. Applications of the ReaxFF to Modeling of Oxygen Diffusion in Y_2O_3-Stabilized ZrO_2

4.1. Diffusion Coefficients. To validate ReaxFF, we performed a series of molecular dynamics (MD) simulations on the oxygen transport processs. These MD simulations started with the three-dimensional YSZ-14 $[(Y_2O_3)(ZrO_2)_6]$ periodic structure obtained from our QM calculations at 0 K. We constructed a $4 \times 4 \times 4$ supercell from this QM-strucutre (736 atoms total) and equilibrated this supercell using ReaxFF NPT calculations at various temperatures (1000, 1250, 1500, 1750, and 2000 K). Then we carried out ReaxFF NVT MD simulations at these temperatures for ∼1 ns. We then used the trajectories generated from these MD simulations to calculate the mean-square displacements (MSD) as a function of the position of each diffusing particle. Figure 8 shows an example trajectory for one of the oxygen atoms in YSZ-14 at 2000 K. Clearly, the oxygen atom is highly mobile with substantial long-range oxygen diffusion.

These ReaxFF MD simulations allow us to calculate diffusion coefficients directly, based on the mean square displacement (MSD), which is calculated as follows:

$$\mathrm{MSD}(m) = \langle |r(t) - r|^2 \rangle = 1/n \sum_{i=1}^{n} |r(m+i) - r(i)|^2$$

where r is the position of the particle, t is the time, k is the total number of snapshots ($k = m{+}n > 0$), m is the maximum number of points allowed for the MSD calculation ($m = k/2$ in

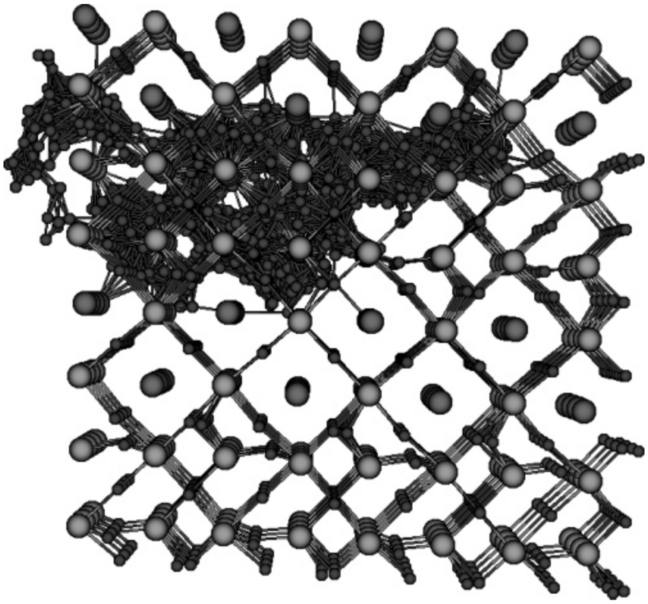

Figure 8. ReaxFF MD simulation: a trajectory of one oxygen atoms in YSZ-14 at $T = 2000$ K, ~400 ps.

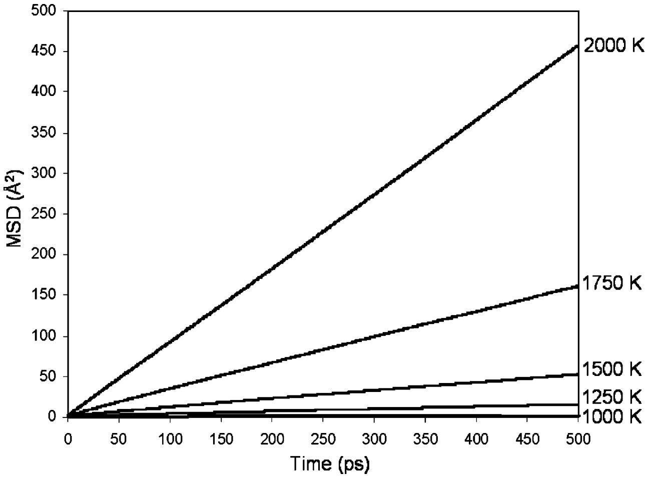

Figure 9. Mean square displacements of oxygen ions in YSZ-14 at various temperatures. The diffusion coefficients extracted from this data are shown in Figure 10.

our calculations), n is the number of data points used for averaging, and i is the step counter. The MSDs of all oxygen atoms at 1000, 1250, 1500, 1750, and 2000 K are shown in Figure 9.

The self-diffusion constant is obtained using the Einstein relation:

$$D = \frac{1}{6Nt}\langle |r(t) - r|^2 \rangle$$

where N is the number of atoms. We fitted the temperature dependence of the diffusion coefficient to

$$D(T) = D_o \exp(-E_a/kT)$$

where E_a is the activation enthalpy. To obtain E_a and D_o, we use the temperature dependence of the diffusion coefficient based on our MD simulations at various temperatures.

Figure 10 shows the calculated and experimental oxygen diffusion coefficients as a function of inverse temperature. The temperature dependences of the oxygen diffusion coefficients show a linear Arrhenius behavior, indicating that there is only one type of the oxygen transport mechanism in YSZ over this range of temperatures.

Although the experiments cover the range from 700 to 1150 K, the MD calculations considered five temperatures from 1000 to 2000 K, eschewing of the lowest temperatures only to reduce the computational effort for these proof-of-concept studies. We will use these methods for much longer calculations in the more complex models of fuel cells. The simulations shown if Figure 10 lead to

$$E_a = 0.90 \text{ eV} \qquad \text{and} \qquad D_o = 2.4 \times 10^{-3} \text{ cm}^{-2}/\text{s}$$

which is in good agreement with the experimental values of

$$E_a = 0.99 \text{ eV} \qquad \text{and} \qquad D_o = 3.4 \times 10^{-3} \text{ cm}^{-2}/\text{s}^{49,50}$$

In particular, Figure 10 shows that extrapolating our higher temperature data to the lower temperatures of the experiments matches reasonably well to the experimental results.

These results indicate that the ReaxFF provides useful predictions for oxygen diffusion within crystalline grains of the YSZ electrolyte.

4.2. Radial Distribution Function. As a first step toward interpreting these results, we calculated the radial distribution functions (RDF) at temperatures of 1000, 1250, 1500, 1750, and 2000 K. Here the RDF is defined as

$$G_{AB}(r) = \frac{g_{AB}(r) \times V}{(N_A N_B - N_{AB})4\pi r^2 \Delta r}$$

where N_A and N_B are the numbers of atoms in groups A and B, respectively, N_{AB} is the number of atoms common to both groups A and B, and V is the unit cell volume. For each case we also plot the integrated number of neighbors up to each radius. This allows us to identify the average coordination for each system.

Figure 11 shows the RDF for the Zr−O, Y−O, O−O, and Y−Zr pair distributions in YSZ-14 at 1000 K (a) and 2000 K (b). Here we see that the average Zr−O bond distance is 2.12 Å in excellent agreement with EXAFS (2.13 Å) and neutron diffraction (2.08 Å) results for YSZ-15.[51,52] The first oxygen shell surrounding Zr goes from ~1.9 Å to ~2.7 Å. This is in very good agreement with synchrotron radiation data, 1.88−2.61 Å.[51]

The RDF for the Y−O pair distributions indicates an average Y−O bond distance of 2.32 Å, again in perfect agreement with experimental EXAFS data, 2.32 Å.[51] The first oxygen shell surrounding Y goes from ~2.0 Å to ~2.5 Å. This is also in very good agreement with results of the synchrotron radiation study, reporting the Y−O distances from 2.07 to 2.43 Å.[51]

Comparing Y−O to Zr−O for the first oxygen shell, we see that our calculations and the experimental results both lead to an average Y−O distance ~0.2 Å longer than the average Zr−O distance, and the corresponding distances for the second oxygen shell are quite similar. This difference between Y−O and Zr−O bond lengths indicates that the geometries of Y and Zr polyhedra are dissimilar so that the ideal fluorite structure does not describe adequately the YSZ atomic arrangement.

The numbers of oxygen atoms surrounding Zr at 1000 K were obtained by integrating the Zr−O RDF up to the first minimum (2.85 Å) past the peak at 2.12 Å, leading to a coordination number $N_{Zr} = 6.9$. Similarly we obtained $N_Y = 5.4$ from integrating the Y−O RDF to the first minimum (2.54 Å) past the peak at 2.32 Å. These values agree with $N_{Zr} = 7.0$ and N_Y

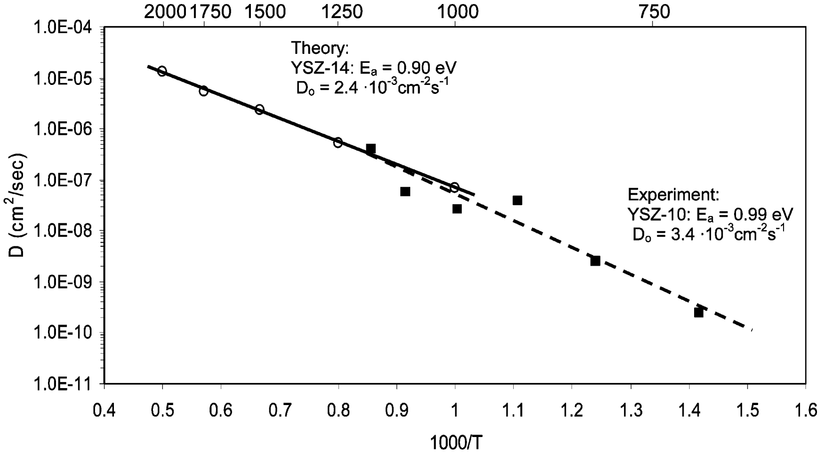

Figure 10. Calculated and experimental YSZ oxygen diffusion coefficients as a function of temperature (top) and 1000/T (bottom).

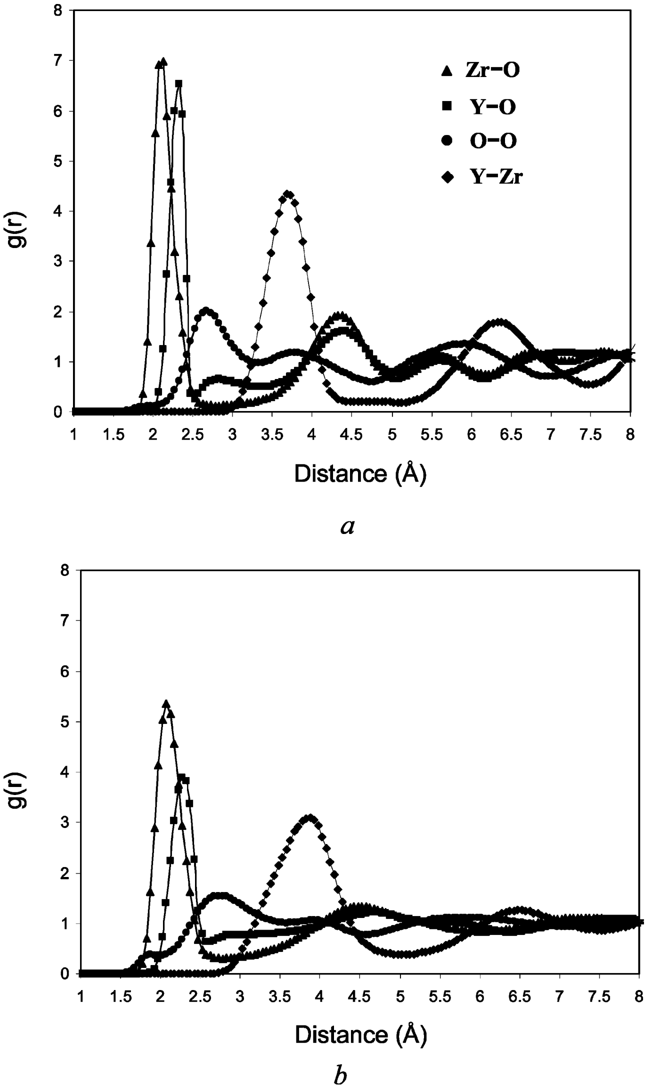

Figure 11. Radial distribution functions for YSZ-14 at 1000 K (a) and 2000 K (b).

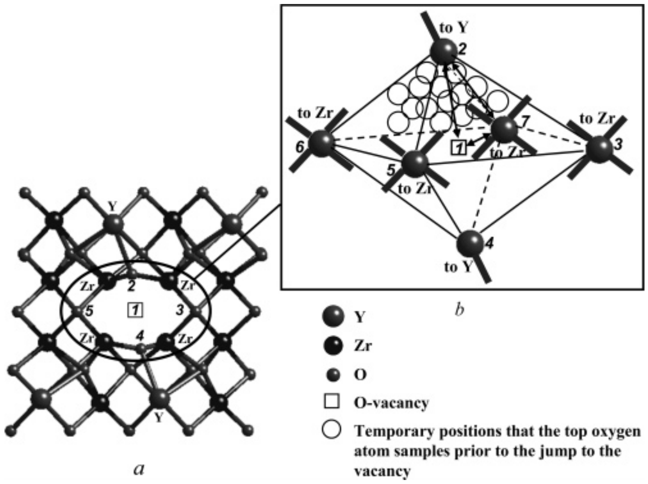

Figure 12. (a) Fragment of the YSZ structure showing a typical oxygen vacancy. (b) Schematic representation of the oxygen diffusion mechanism in YSZ (only oxygen atoms are shown).

= 5.9 extracted by combining synchrotron radiation and EXAFS studies.[51] The coordination number $N_{Zr} = 6.9$ is very close to the coordination $N_{Zr} = 7.0$ in the monoclinic phase of ZrO_2, and $N_Y = 5.4$ is only slightly lower than the coordination number $N_Y = 6$ in cubic Y_2O_3. Indeed, our initial structure for YSZ had $N_Y = 8$ with all Y atoms starting at 2NN positions with respect to the O vacancies. However, during the MD simulation the coordination number of Y, if it is based only on the RDF peak at 2.32 Å, would decrease from 8 to 5.4, indicating that some oxygens surrounding Y have moved away from the Y cations toward the vacancies. This results in configurations in which

(1) some of the Y atoms are in NN positions to vacancies and

(2) some of the Y−O bonds are stretched.

The small, broad peak observed in the RDF at 2.8 Å, just beyond the peak at 2.32 Å corresponding to the first oxygen shell of Y, most probably reflects this rearrangement of the O atoms. Including this second peak in the first oxygen shell of Y increases the coordination number from 5.4 to 7.9, very close to the initial coordination number of 8.

Analyzing the RDF for the O−O pair distributions in YSZ-14 at 1000 and 2000 K, we see that the average O−O bond distance is ~2.67 Å at 1000 K, increasing to ~2.77 Å at 2000 K. The average oxygen has six oxygen neighbors in the first O−O coordination shell, which is the same as in ZrO_2 and Y_2O_3 (considering only O−O distances less than 3 Å).

At 2000 K, the O−O RDF has a small peak (0.2 atoms) at 1.9 Å (Figure 11b); no such peak occurs for 1000 K. To understand the origin of such unexpectedly short distances, we examined the trajectory to learn how they arose. A typical case is shown in Figure 12. Here the vacancy is numbered as *1* and the six oxygen atoms nearest the vacancy are numbered *2*−*7*. If there was no vacancy, the *2*−*4*, *3*−*6*, and *5*−*7* distances going across *1* would all be ~5.2 Å, but because of the vacancy, the

2−*4* distance relaxes to ∼3.3 Å and *3*−*6* and *4*−*7* stay at ∼5.2 Å. What is special about *2*−*4* is that *2* is bonded to Y as is *4*. Thus, position *1* is a 2NN to both Y. In the dynamics the O atom in position *2* jumped to position *1*. Immediately after jumping, the new *1*−*4* distance is ∼1.9 Å for ∼0.025 ps (1 frame in our analysis trajectory) and then the atoms relax so that the frame 0.025 ps later has the *1*−*4* distance of ∼2.6 Å, as are the new *1*−*3*, *1*−*5*, *1*−*6*, and *1*−*7* distances.

All RDF peaks in Figure 11 broaden with increasing temperature, mainly due to thermal expansion, but even at 2000 K all peaks, including those corresponding to the O−O pair distribution, remain resolved. This provides evidence that the oxygen diffusion in YSZ can be considered as hopping between relatively well-defined positions, rather than diffusion through a liquid-like medium. This allows us to analyze the diffusion in terms of the motion of the O vacancy as discussed below.

4.3. Oxygen Diffusion Mechanism. Many previous experimental and computational works on YSZ (see, for instance,[53−56]) found that oxygen vacancies are more likely located in NN positions to Zr. Oxygen vacancies close to two Y stabilizer ions are "trapped" so that oxygen ion hopping between two stabilizer ions is not possible. In contrast, some other works on YSZ[57−59] state that there is no preferential ordering or association of the oxygen vacancies.

Our initial YSZ structure was based on our QM calculations, with all O vacancies close to Zr and in 2NN positions with respect to the Y stabilizer ions (see Figure 12a). However, our ReaxFF MD simulations show that some vacancies jump from their 2NN positions to NN positions to Y, as mentioned above in section 4.2. Here we provide a more detailed description of the possible oxygen diffusion mechanism in YSZ.

Oxygen sites in YSZ are arranged inside the cation sublattice, which contains two types of cation polyhedra: tetrahedra and octahedra. According to ref 56, almost all oxygens (97%) occupy positions inside the tetrahedron spaces (regular positions) and only about 3% of the oxygen ions jump temporarily inside the octahedra (interstitial positions) during the diffusion process. Therefore, the oxygen migration mostly occurs between adjacent tetrahedra. A detailed analysis of possible first neighboring cation arrangements (including all possible Y and Zr distributions) around the oxygen atoms and how these arrangements influence on the oxygen diffusion is in refs 60 and 61. Our results agree with those obtained in refs 56, 60, and 61.

In addition to the cation neighbors, each O vacancy is surrounded by six O atoms forming the first O−O coordination shell of the vacancy (Figure 12b). There are two distinct pathways for oxygen diffusion in YSZ:

- In the first path, the vacancy goes close to Zr while remaining a 2NN to Y (in Figure 12b it is, for example, a jump from *1* to *7*). In this case, the diffusion process consists of two types of vacancy jumps: inter- and intra-Zr polyhedra hopping. During this hopping some Zr polyhedra may change the 6-fold coordination for the polyhedron containing the vacancy to 7-fold and vice versa, but the coordination number of the average Zr remains ∼7 as for the initial YSZ structure. This is exactly what we observe in our RDFs.

- The second path allows oxygen atoms belonging to the Y polyhedron to jump to the vacancy so that the vacancy moves from the 2NN to the NN position to the Y (in Figure 12b this is a jump from *1* to *2*). In this case, the diffusing O no longer belongs to the Y polyhedron, so that the coordination number of the average Y decreases. This situation was already discussed above in section 4.2. The analysis of the RDF and *N*, shows that more than one Y−O bond can elongate significantly. Therefore, the Y polyhedra in YSZ change more during the O diffusion, than do the Zr polyhedra.

Indeed, we find that the oxygen diffusion in YSZ combines both pathways (for instance, the vacancy first jumps from *1* to *7* and then from *7* to *2*), leading to the following description. O atoms next to a vacancy spend ∼70 ps (at 1500 K) in an oscillatory motion towards the vacancy (in Figure 12b this motion is shown by empty spheres) before one of them finally succeeds in jumping there. Even after jumping, the oxygen may jump back into the former position. Such local fluctuations forth and back (local diffusion) do not contribute to the long-range oxygen diffusion in YSZ. However, long-range oxygen diffusion also occurs. In the latter case, the vacancy, after the local diffusion step, hops to one of the NN oxygen positions, and does not return to the initial position. Instead, after some fluctuations the vacancy jumps to a new position that is now a 2NN to the initial vacancy position. Then all steps described above are reiterated, finally resulting in long-range oxygen diffusion in YSZ.

The above discussion shows that during the oxygen diffusion, many configurations are found in which one of the two Y atoms occupies a NN position to the O vacancy while the other is in a 2NN position (NN-2NN) and there are others in which both Y atoms occupy 2NN positions to the O vacancy (2NN-2NN). However, the NN−NN configuration (both Y atoms are in NN positions to the O vacancy) is *not* favorable. According to our QM calculations the energy for this NN−NN configuration is ∼0.7 eV higher than the NN-2NN or 2NN-2NN configuration. Also the barrier for the oxygen migration between two Y NN atoms (the Y−Y edge) is 2.04 eV, which is significantly higher than the barrier along the Zr−Y edge, 0.85 eV.[60] Other configurations, such as NN-3NN, 2NN-3NN, 3NN-3NN, *etc*. (some of them are mentioned in section 3), can also be realized in process of the oxygen diffusion in YSZ. The difference in energies for these observed configurations does not exceed 0.5 eV. Examining our ReaxFF MD trajectories for possible diffusion pathways, we conclude that oxygen ion transport occurs primarily along the [100] direction, which agrees with some previous theoretical and experimental studies (for example, refs 49, 60, 62, and 63).

5. Conclusions

We report the development of the ReaxFF reactive force field for the YSZ oxide-ion conductor. It is based on substantial data derived from QM calculations on clusters and periodic systems.

We also report ReaxFF MD studies of the oxygen migration properties of YSZ. The predicted oxygen diffusion coefficients in YSZ as a function of temperature were used to extract the activation energy for oxygen transport. The values for both the diffusion coefficient and the activation energy are in excellent agreement with experimental data. This validates the use of ReaxFF for such problems.

These results indicate that ReaxFF properly describes the oxygen migration properties and structural characteristics of YSZ. Currently, we are in the process of combining this YSZ force field with the ReaxFF describing the chemistry on Pt and Ni surfaces. This will allow us to simulate the complex chemical processes at the anode/electrolyte interfaces in a SOFC.[24] This would enable first principles predictions on the chemical processes at the triple-phase boundaries of fuel cells.

Acknowledgment. This work was supported by the Department of Defense Multidisciplinary University Research Initiative (MURI) program administered by the Office of Naval Research under grant N00014-02-1-0665 (Program manager Michele Anderson). In addition, some support was provided by DOE-FETL (DE-FC26-02NT41631, program manager Lane Wilson). We thank Professors Sossina Haile and David Goodwin for helpful discussions. The facilities of the MSC used in these studies were established with grants from DURIP-ONR, DURIP-ARO, and NSF-MRI. Additional support for the MSC comes from ONR, ARO, DOE, NSF, NIH, Chevron, Nissan, Dow Corning, Intel, Pfizer, Boehringer-Ingelheim, and Allozyne.

Supporting Information Available: ReaxFF parameters developed in this paper, tables of the energies used in Figures 2−7, and the bgf-file for the final configuration from the dynamics of the YSZ-14 structure at 1000 K. This information is available free of charge via the Internet at http://pubs.acs.org.

References and Notes

(1) Etsell, T. H.; Flengas, S. N. *Chem. Rev.* **1970**, *70*, 339.

(2) Steele, D.; Fender, B. E. F. *J. Phys. C* **1974**, *7*, 1.

(3) Roth, W. L.; Wong, R.; Goldman, A. I.; Canova, E.; Kao, Y. H.; Dunn, B. *Solid State Ionics* **1986**, 18−19, 1115.

(4) Tuilier, M. H.; Dexpert-Ghys, J.; Dexpert, H.; Lagarde, P. *J. Solid State Chem.* **1987**, *69*, 153.

(5) Morikawa, H.; Shimizugawa, Y.; Marumo, F.; Harasawa, T.; Ikawa, H.; Tohji, K.; Udagawa, Y. *J. Ceram. Soc. Jpn* **1988**, *96*, 253.

(6) Weller, M. Z. *Metallkd* **1993**, *84*, 6.

(7) Catlow, C. R. A.; Chadwick, A. V.; Greaves, G. N.; Moroney, L. M. *J. Am. Ceram. Soc.* **1986**, *69*, 272.

(8) Veal, B. W.; McKale, A. G.; Paulinkas, A. P.; Rothman, S. J.; Nowicki, L. G. *Physica B* **1988**, *150*, 234.

(9) Komyoji, D.; Yoshiasa, A.; Moriga, T.; Emura, S.; Kanamura, F.; Koto, K. *Solid State Ionics* **1992**, *50*, 291.

(10) Li, P.; Chen, W.; Penner-Hahn, J. E. *J. Am. Ceram. Soc.* **1994**, *77*, 118.

(11) Butler, V.; Catlow, C. R. A.; Fender, B. E. F. *Solid State Ionics* **1981**, *5*, 539.

(12) Mackrodt, W. C.; Woodrow, P. M. *J. Am. Ceram. Soc.* **1986**, *69*, 277.

(13) Dewhurst, J. K.; Lowther, J. E. *Phys. Rev. B* **1988**, *57*, 741.

(14) Stapper, G.; Bernasconi, M.; Nicoloso, N.; Parrinello, M. *Phys. Rev. B* **1999**, *59*, 797.

(15) Jomard, J.; Petit, T.; Pasturel, A.; Magaud, L.; Kresse, G.; Hafner, J. *Phys. Rev. B* **1999**, *59*, 4044.

(16) Ostanin, S. A.; Salamatov, E. I. *JETP Lett.* **2001**, *74*, 552.

(17) van Duin, A. C. T.; Dasgupta, S.; Lorant, F.; Goddard, W. A., III. *J. Phys. Chem. A* **2001**, *105*, 9396.

(18) Strachan, A.; van Duin, A. C. T.; Chakraborty, D.; Dasgupta, S.; Goddard, W. A., III. *Phys. Rev. Lett.* **2003**, *91*, 098301.

(19) Strachan, A.; Kober, E. M.; van Duin, A. C. T.; Oxgaard, J.; Goddard, W. A., III. *J. Chem. Phys.* **2005**, *122*, 054502.

(20) van Duin, A. C. T.; Zeiri, Y.; Dubnikova, F.; Kosloff, R.; Goddard, W. A., III. *J. Am. Chem. Soc.* **2005**, *127*, 11053.

(21) Chenoweth, K.; Cheung, S.; van Duin, A. C. T.; Goddard, W. A., III; Kober, E. M. *J. Am. Chem. Soc.* **2005**, *127*, 7192.

(22) Goddard, W. A., III; van Duin, A. C. T.; Chenoweth, K.; Cheng, M. J.; Pudar, S.; Oxgaard, J.; Merinov, B.; Jang, J. H.; Persson, P. *Top. Catal.* **2006**, *38*, 93.

(23) Goddard, W. A., III; Merinov, B.; van Duin, A. C. T.; Jacob, T.; Blanco, M.; Molinero, V.; Jang, S. S.; Jang, Y. H. *Mol. Simul.* **2006**, *32*, 251.

(24) Buehler, M. J.; van Duin, A. C. T.; Goddard, W. A., III. *Phys. Rev. Lett.* **2006**, *96*, 095505.

(25) Ludwig, J.; Vlachos, D. G.; van Duin, A. C. T.; Goddard, W. A. *J. Phys. Chem. B* **2006**, *110*, 4274.

(26) Cheung, S.; Deng, W. Q.; van Duin, A. C. T.; Goddard, W. A. *J. Phys. Chem. A* **2005**, *109*, 851.

(27) Nielson, K. D.; van Duin, A. C. T.; Oxgaard, J.; Deng, W. Q.; Goddard, W. A. *J. Phys. Chem. A* **2005**, *109*, 493.

(28) Zhang, Q.; Cagin, T.; van Duin, A. C. T.; Goddard, W. A.; Qi, Y.; Hector, L. G. *Phys. Rev. B* **2004**, *69*, 045423.

(29) Chenoweth, K.; van Duin, A. C. T.; Goddard, W. A. Submitted to *J. Am. Chem. Soc.*

(30) Nakano, A.; Kalia, R. K.; Nomura, K.; Sharma, A.; Vashista, P.; Shimojo, F.; van Duin, A. C. T.; Goddard, W. A.; Biswas, R.; Srivastava, D. *Comput. Mater. Sci.* **2007**, *38*, 642.

(31) Ceperley, D. M.; Alder, B. J. *Phys. Rev. Lett.* **1980**, *45*, 566.

(32) Perdew, J. P.; Zunger, A. *Phys. Rev. B* **1981**, *23*, 5048.

(33) Kohn, W.; Sham, L. J. *Phys. Rev.* **1965**, *140*, A1133.

(34) Perdew, J. P.; Burke, K.; Ernzerhof, M. *Phys. Rev. Lett.* **1996**, *77*, 3865.

(35) Slater, J. C. Quantum Theory for Molecules and Solids. In *The Self-Consistent Field for Molecules and Solids*; McGraw-Hill: New York, 1974; Vol. 4.

(36) Becke, A. D. *Phys. Rev. A* **1988**, *38*, 3098.

(37) Vosko, S. H.; Wilk, L.; Nusair, M. *Can. J. Phys.* **1980**, *58*, 1200.

(38) Lee, A.; Yang, W.; Parr, R. G. *Phys. Rev. B* **1988**, *37*, 785.

(39) Koch W.; Holthausen, M. C. *A Chemist's Guide to Density Functional Theory*; Wiley-VCH: Weinheim, 2001.

(40) Mattsson, A. E.; Schultz, P. A.; Desjarlais, M. P.; Mattsson, T. R.; Leung, K. *Modelling Simul. Mater. Sci. Eng.* **2005**, *13*, R1.

(41) Jaguar 4.2, Schrödinger Inc., Portland, OR. See, for example: Greeley, B. H.; Russo, T. V.; Mainz, D. T.; Friesner, R. A.; Langlois, J.-M.; Goddard, W. A., III; Donnelly, R. E.; Ringnalda, M. N. *J. Chem. Phys.* **1994**, **2000.** *101*, 4028.

(42) Hay, P. J.; Wadt, W. R. *J. Phys. Chem.* **1985**, *82*, 299.

(43) Goddard, W. A., III. *Phys. Rev.* **1968**, *174*, 659.

(44) Melius, C. F.; Goddard, W. A., III. *Phys. Rev. A* **1974**, *10*, 1528.

(45) Francl, M. M.; Pietro, W. J.; Hehre, W. J.; Binkley, J. S.; Gordon, M. S.; DeFrees, D. J.; Pople, D. J. *J. Chem. Phys.* **1982**, *77*, 3654.

(46) Schultz, P. A. unpublished (a description of the method is in: Feibelman, P. *J. Phys. Rev. B* **1987**, 35, 2626].

(47) Schultz, P. A. unpublished; see http://dft.sandia.gov/Quest.

(48) Troullier, N.; Martins, J. L. *Phys. Rev B* **1991**, *43*, 1993.

(49) Kilo, M.; Argirusis, C.; Borchardt, G.; Jackson, R. *Phys. Chem. Chem. Phys.* **2003**, *5*, 2219.

(50) Minh, N. Q. *J. Am. Ceram. Soc.* **1993**, *76*, 563.

(51) Ishizawa, N.; Matsushima, Y.; Hayashi, M.; Ueki, M. *Acta Crystallogr., Sect. B* **1999**, *55*, 726.

(52) Kaiser-Bischoff, I.; Boysen, H.; Frey, F.; Hoffmann, J.-U.; Hohlwein, D.; Lerch, M. *J. Appl. Crystallogr.* **2005**, *38*, 139.

(53) Li, P.; Chen, I.; Penner-Hahn, J. E. *Phys. Rev. B* **1993**, *48*, 10063.

(54) Catlow, C. R. A.; Chadvick, A. V.; Greaves, G. N.; Moroney, L. M. *J. Am. Ceram. Soc.* **1986**, *69*, 272.

(55) Khan, M. S.; Islam, M. S.; Bates, D. R. *J. Mater. Chem.* **1998**, *8*, 2299.

(56) Yamamura, Y.; Kawasaki, S.; Sakai, H. *Solid State Ionics* **1999**, *126*, 181.

(57) Shimojo, F.; Okabe, T.; Tachibana, F.; Kobayashi, M.; Okazaki, H. *J. Phys. Soc. Jpn.* **1992**, *61*, 2848.

(58) Shimojo, F.; Okazaki, H. *J. Phys. Soc. Jpn.* **1992**, *61*, 4106.

(59) Kilo, M.; Jackson, R. A.; Borchardt, G. *Philos. Mag.* **2003**, *11*, 3309.

(60) Devanathan, R.; Weber, W. J.; Singhal, S. C.; Gale, J. D. *Solid State Ionics* **2006**, *177*, 1251.

(61) Pornprasertsuk, R.; Ramanarayanan, P.; Musgrave, C. B.; Prinz, F. B. *J. Appl. Phys.* **2005**, *98*, 103513.

(62) Horiuchi, H.; Schultz, A. J.; Leung, P. C. W.; Williams, J. M. *Acta Crystallogr. B* **1984**, *49*, 367.

(63) Kaiser-Bischoff, I.; Boysen, H.; Scherf, C.; Hansen, T. *Phys. Chem. Chem. Phys.* **2005**, *7*, 2061.